Physica B 625 (2022) 413452

Contents lists available at ScienceDirect

Physica B: Physics of Condensed Matter

journal homepage: www.elsevier.com/locate/physb

Time dependent thermal transport through a strongly correlated plexcitonic nanojunction

A. Goker

Department of Physics, Bilecik University, 11210, Gulumbe, Bilecik, Turkey

ARTICLE INFO

Keywords:
Kondo effect
Vibrational effects
Tunnelling
Plasmonics

ABSTRACT

We investigate the implications of the sinusoidal modulation of the higher energy level of a Coulomb blockaded quantum emitter, composed of two discrete energy levels under strong electron–phonon coupling and coupled to metallic nanoparticles possessing plasmon resonances, on the evolution of entropy current through the nanojunction by invoking the time dependent non-crossing approximation. The ensuing time dependent entropy current exhibits sinusoidal oscillations with the driving frequency. The amplitude of oscillations remains more or less constant in low bias regime but gets suppressed in high bias regime for fixed electron–phonon coupling. Boosting the electron–phonon coupling quenches the amplitude of oscillations in low bias regime. The amplitude of the oscillations increases upon reducing the driving frequency in low bias regime. We discuss these results with the aid of a microscopic model.

1. Introduction

The Holy Grail of nanotechnology has long been to design and develop next generation miniature optoelectronic devices that can beat the notorious diffraction limit and overcome the Moore's law [1,2]. Unprecedented tunability of the surface plasmon polariton (SPP) resonances of noble metal nanoparticles provided a great opportunity to achieve this feat by enabling to concentrate the energy of the illumination into tiny regions that are even smaller than the wavelength of light [3,4].

The plasmon resonances of metal nanoparticles induce large electromagnetic field enhancements [5], which enable coupling with nearby quantum emitters. Strong coupling of plasmons with the resonant excitations in the quantum emitter yields plexcitons, hybrid light-matter modes. The interaction between the participating modes in a plexciton induces perturbations which enable to improve the poor quality factor (Q) resonances arising due to the inherent absorption losses of metals [6]. Therefore, plexcitons constitute an indispensable tool for novel molecular optoelectronic devices [7] as well as surface catalytic reactions [8].

Enhancement of the solar energy harvesting via SPP is another issue under active investigation[9–11]. This technology exploits the absorption of the sunlight by a plasmonic metal nanoparticle, which then transfers the captured energy to a semiconductor via dipole–dipole coupling [12,13]. The semiconductor converts this energy into electron–hole pairs near its conduction and valence bands. The biggest hurdle for the plasmon enhanced resonant energy transfer is the much shorter lifetime of the plasmon compared with the electron–hole pairs in a dye or quantum dot [14].

There have been several previous theoretical attempts to explore the behaviour of plexcitonic nanojunctions with single or multiple quantum emitters [15–18]. However, a realistic description of a plexcitonic junction was still lacking because these studies ignored spin effects and strong Coulomb interaction within the quantum emitter. As a first step towards developing a proper quantum model, the Green function method has been deployed [19]. It revealed that only the dipolar plasmon mode is relevant in the strong coupling regime. Combination of the first principles methods and finite element simulations demonstrated that the metal plasmons enhance the weak charge transfer exciton in the 2H lateral and van der Waals MoS_2/WS_2 heterostructures [20].

The electron correlations within the quantum emitter have been explored previously by employing the Green function method and the non-crossing approximation to study the evolution of the optical emission spectrum [21], the electrical conductance [22] and the entropy current due to a temperature gradient between the metal nanoparticles [23,24]. The entropy current represents a fundamental concept that quantifies the heat flow through the nanojunction, which stems from the conversion of the impinging optical energy into thermal energy. Since a photovoltaic device operates intrinsically as a heat engine, it is imperative to develop an accurate quantum thermodynamics model to describe its behaviour.

In this paper, we will study for the first time the dynamical evolution of the entropy current through a plexcitonic nanojunction by

E-mail address: aihsan.goker@bilecik.edu.tr.

https://doi.org/10.1016/j.physb.2021.413452
Received 4 August 2021; Received in revised form 7 September 2021; Accepted 28 September 2021
Available online 14 October 2021

taking into account the vibrational and strong electron correlation effects within the quantum emitter. This represents a new paradigm compared to earlier studies focusing on electrical conductance through a single quantum dot [25]. We will also put forward an intuitive scenario which adequately explains the results of intricate numerical many-body calculations. In this manner, we strive to sketch a fairly realistic quantum thermodynamics picture of a continuously modulated plexcitonic nanojunction.

2. Method

Our analysis will focus on a nano junction composed of a quantum emitter with two discrete states placed between two metal nanoparticles and a laser beam which excites this system. It is possible to envisage the quantum emitter as a double quantum dot. The Hamiltonian which models this nano junction can be written as

$$H = H_N + H_{EN} + \sum_{\alpha\in\{E,rad\}} (H_\alpha + V_\alpha). \tag{1}$$

The first piece H_N represents the metal nanoparticles such that

$$H_N = \sum_{K\in\{L,R\},\sigma} \varepsilon_{K\sigma} c^\dagger_{K\sigma} c_{K\sigma} + \sum_{K\in\{L,R\}} \varepsilon_{pK} b^\dagger_K b_K, \tag{2}$$

while the second piece H_{EN} captures the plasmon–exciton coupling

$$H_{EN} = \sum_{K\in\{L,R\},\sigma} \left(\Delta_K c^\dagger_{e\sigma} c_{g\sigma} b_K + h.c.\right). \tag{3}$$

The quantum emitter is modelled by H_E

$$H_E = \sum_{s\in\{g,e\},\sigma} \left[\varepsilon_s + \lambda(d + d^\dagger)\right] c^\dagger_{s\sigma} c_{s\sigma} + \omega_0 d^\dagger d + J\sum_\sigma \left(c^\dagger_{g\sigma} c_{e\sigma} + h.c.\right) + \frac{U}{2}\sum_{s\in\{g,e\}} n_{s\sigma} n_{s\sigma'}, \tag{4}$$

and V_E amounts to shuttling of electrons between the discrete states of quantum emitter and the metal nanoparticles

$$V_E = \sum_{K\in\{L,R\},\sigma} \left(V_{K,g(e)} c^\dagger_{K\sigma} c_{g(e)\sigma} + h.c.\right). \tag{5}$$

The hopping amplitude between the discrete states of the quantum emitter and the metal nanoparticles is defined as

$$\begin{aligned} \bar{\Gamma} &= \bar{\Gamma}_{L,g} = 2\pi |V_{L,g}(\varepsilon_f)|^2 \\ \bar{\Gamma} &= \bar{\Gamma}_{R,e} = 2\pi |V_{R,e}(\varepsilon_f)|^2 \end{aligned} \tag{6}$$

along with $\Gamma = \bar{\Gamma}\rho(\varepsilon_f)$. Here, $\rho(\varepsilon_f)$ denotes the density of states at Fermi level of the metal nanoparticles ε_f. In order to arrive at these expressions, we assume that the tunnelling terms are time and energy independent such that $V_{K,g(e)}(\varepsilon) = V_{K,g(e)}(\varepsilon_f)$. Furthermore, the left nanoparticle is only coupled to the lower lying discrete state $|g\rangle$ and the right nanoparticle is only coupled to the higher lying discrete state $|e\rangle$. This is meant to prevent tunnelling between the metal nanoparticles via a single discrete level and can be achieved experimentally by placing the quantum emitter asymmetrically in the junction. Finally, the coupling of each discrete level with the relevant metal nanoparticle is taken to be equal, i.e. $V_{L,g} = V_{R,e}$.

The laser radiation is incorporated with

$$H_{rad} = \sum_\alpha \varepsilon_\alpha a^\dagger_\alpha a_\alpha \tag{7}$$

and the coupling between the laser radiation and the plasmon modes is

$$V_{rad} = \sum_{K\in\{L,R\},\alpha} \left(W_{\alpha,K} a^\dagger_\alpha b_K + h.c.\right). \tag{8}$$

In this model, the quantum emitter, which contains two spin degenerate levels $|g\rangle$ and $|e\rangle$, exhibits an energy gap with magnitude $|\varepsilon_e - \varepsilon_g|$. In each level, $c^\dagger_{s\sigma}(c_{s\sigma})$ create(destroy) an electron with spin σ while $c^\dagger_{K\sigma}(c_{K\sigma})$ is the counterpart for free fermions in the metal nanoparticles. $b^\dagger_K(b_K)$ is the bosonic operator that creates(annihilates) the plasmon with energy ε_{pK} in the left and right nanoparticles with $K = L, R$ while ε_α stands for the energy of the laser radiation in mode α. J is the amplitude of electron transfer between $|g\rangle$ and $|e\rangle$ while $V_{K,g(e)}$ denotes the coupling amplitude between the metal nanoparticles and $|g(e)\rangle$. $W_{\alpha,K}$ denotes the interaction energy between the laser radiating in mode α and the dipolar plasmon modes of each nanoparticle. Δ_K corresponds to the strength of the coupling between the dipolar plasmon modes of the left or right metal nanoparticle and the exciton formed in the quantum emitter. Finally, λ denotes the strength of the electron–phonon coupling with $d^\dagger(d)$ creating (destroying) a phonon localized within the quantum emitter while ω_0 stands for the phonon energy.

The strong electron–phonon coupling regime, where λ is on the same order with Γ, can be dealt with Lang–Firsov unitary transformation [26]. This transformation turns the Hamiltonian corresponding to the quantum emitter into [24]

$$\bar{H}_E = \sum_{s\in\{g,e\},\sigma} \left(\varepsilon_s - \frac{\lambda^2}{\omega_0}\right) c^\dagger_{s\sigma} c_{s\sigma} + \omega_0 d^\dagger d + J\sum_\sigma \left(c^\dagger_{g\sigma} c_{e\sigma} + h.c.\right) + \left(\frac{U}{2} - \frac{2\lambda^2}{\omega_0}\right) \sum_{s\in\{g,e\}} n_{s\sigma} n_{s\sigma'}, \tag{9}$$

which gives rise to the renormalization of the quantum emitter levels and the Hubbard interaction as $\bar{\varepsilon}_s = \varepsilon_s - \lambda^2/\omega_0$ and $\bar{U} = U/2 - (2\lambda^2/\omega_0)$ respectively.

Due to the tight confinement of electrons within the quantum emitter, the renormalized Hubbard interaction is still far larger than the linewidth of each discrete level, leading to $\bar{U} \to \infty$ in practice. This forbids the double occupancy of discrete levels. In this case, the original electron operators can be decomposed into massless boson and pseudofermion operators as

$$\begin{aligned} c_{g(e)\sigma} &= b^\dagger_{g(e)} f_{g(e)\sigma} \\ c^\dagger_{g(e)\sigma} &= f^\dagger_{g(e)\sigma} b_{g(e)}, \end{aligned} \tag{10}$$

satisfying

$$Q_{B,g(e)} = b^\dagger_{g(e)} b_{g(e)} + \sum_\sigma f^\dagger_{g(e)\sigma} f_{g(e)\sigma} = 1, \tag{11}$$

so that the standard diagrammatic techniques can still be applied. Consequently, the Hubbard term can safely be omitted. This procedure converts $\bar{H}_E$ into

$$\bar{H}_E = \sum_{s\in\{g,e\},\sigma} \bar{\varepsilon}_s c^\dagger_{s\sigma} c_{s\sigma} + \omega_0 d^\dagger d + J\sum_\sigma \left(c^\dagger_{g\sigma} c_{e\sigma} + h.c.\right), \tag{12}$$

and $\bar{V}_E$ is casted as

$$\bar{V}_E = \sum_{K\in\{L,R\},\sigma} \left(\tilde{V}_{K,g(e)} c^\dagger_{K\sigma} b^\dagger_{g(e)} f_{g(e)\sigma} + h.c.\right) \tag{13}$$

where $\tilde{V}_{K,g(e)} = V_{K,g(e)} exp\left[-\frac{\lambda^2}{\omega_0^2}(N_{ph} + \frac{1}{2})\right]$ with $N_{ph} = \frac{1}{exp\left(\frac{\hbar\omega_0}{k_B T}\right)-1}$. We will refer to $\frac{\lambda^2}{\omega_0}$ as V_{e-p} hereafter.

Further approximations are needed to be able to tackle this Hamiltonian. First, the pump laser is taken to be aligned perpendicular to the axis which connects the metal nanoparticles to ensure that they absorb the photons in the same phase[23,27]. Moreover, a single mode laser with energy ε_0 pumps only the dipolar plasmon mode of the metal nanoparticles and laser beam's excitation of the quantum emitter is ignored. This allows to omit the term involving J in H_E. In this case, it is legitimate to take equal dipolar plasmon energy for each nanoparticle such that $\varepsilon_{pL} = \varepsilon_{pL} = \varepsilon_p$ as well as symmetrical plasmon–exciton and plasmon–laser couplings $\Delta_L = \Delta_R = \Delta$ and $W_{0,L} = W_{0,R} = W_0$. Finally, it is possible to adjust the intensity of the laser beam along the axis or one of the metal nanoparticles can be picked in a slightly different size to achieve a temperature gradient between them experimentally.

We start with the fundamental definition of entropy

$$dS = dQ/T, \tag{14}$$

where dQ corresponds to the differential heat flow and T denotes the temperature. Taking the time derivative of both sides gives the entropy current I^s. We can define the entropy current across this particular nanojunction in terms of the energy ($I^E_{L(R)}$, I^E_γ) and particle currents ($I_{L(R)}$, I_γ) as [24]

$$I^s = \frac{I^E_L - \mu_L I_L}{T_L} + \frac{I^E_R - \mu_R I_R}{T_R} + \frac{I^E_\gamma - \mu_\gamma I_\gamma}{T_\gamma}, \tag{15}$$

where, the nominators amount to definition of the heat current, $dQ/dt = KA\Delta T$. In this expression, K represents the thermal conductivity, A stands for the cross section of the junction while ΔT denotes the temperature gradient across the junction. Consequently, the entropy current is directly related to the thermal conductivity, which can be directly measured experimentally [28,29]. In Eq. (15), the terms on the right denote the left(L), right(R) metal nanoparticles and the photon bath (γ) respectively. Since the photon bath and the quantum emitter are not coupled, the third term is zero. Its effect is accounted for by the plasmon Green functions.

The relevant components of the particle current can be expressed in terms of the non-equilibrium Green functions as

$$I_{Lg}(t) = -2\bar{\Gamma} Re \int_{-\infty}^{t} dt_1 G^<_g(t,t_1) e^{\phi(t-t_1)} b_g(t_1,t) h(t-t_1)$$
$$+ 2\bar{\Gamma} Re \int_{-\infty}^{t} dt_1 (g_g(t,t_1) B^<_g(t_1,t) + G^<_g(t,t_1) e^{\phi(t-t_1)}$$
$$b_g(t_1,t)) f_L(t-t_1) \tag{16}$$

and

$$I_{Re}(t) = -2\bar{\Gamma} Re \int_{-\infty}^{t} dt_1 G^<_e(t,t_1) e^{\phi(t-t_1)} b_e(t_1,t) h(t-t_1)$$
$$+ 2\bar{\Gamma} Re \int_{-\infty}^{t} dt_1 (g_e(t,t_1) B^<_e(t_1,t) + G^<_e(t,t_1) e^{\phi(t-t_1)}$$
$$b_e(t_1,t)) f_R(t-t_1), \tag{17}$$

where

$$h(t-t_1) = \int_{-D}^{D} \frac{d\varepsilon}{2\pi} \rho(\varepsilon) e^{i\varepsilon(t-t_1)}, \tag{18}$$

$$f_L(t-t_1) = \int_{-D}^{D} \frac{d\varepsilon}{2\pi} \rho(\varepsilon) \frac{e^{i\varepsilon(t-t_1)}}{1 + e^{\beta_L(\varepsilon - V/2)}} \tag{19}$$

and

$$f_R(t-t_1) = \int_{-D}^{D} \frac{d\varepsilon}{2\pi} \rho(\varepsilon) \frac{e^{i\varepsilon(t-t_1)}}{1 + e^{\beta_R(\varepsilon + V/2)}}. \tag{20}$$

The corresponding energy currents are obtained by multiplying the integrands for $h(t-t_1)$, $f_L(t-t_1)$ and $f_R(t-t_1)$ with ε. In these expressions $\rho(\varepsilon)$ stand for the density of states of the metal nanoparticles, while $\beta_{L(R)}$ and V denote the inverse temperature of the metal nanoparticles and the bias voltage respectively.

3. Results and discussion

In this paper, we will consider a scenario, where ε_g is kept stationary, while ε_e is sinusoidally modulated via a gate voltage such that

$$\varepsilon_e(t) = \varepsilon_e(0) + A cos(\omega t). \tag{21}$$

Our calculations will pertain to $\varepsilon_e(0)$ = -2.0 eV, ε_g = -4.8 eV and A = 0.4 eV so that the initial steady state of the quantum emitter is identical to the case studied previously [24]. We will analyze the influence of driving frequency ω, ambient temperature T, voltage bias V and electron–phonon coupling strength V_{e-p} on the ensuing entropy current through the nanojunction. Since the Fermi level of the metal nanoparticles ε_f is taken to be zero, this set of parameters put both $|g\rangle$ and $|e\rangle$ well below ε_f in Coulomb blockade, which means that the quantum transport is prevented across this junction. However, a mechanism to overcome this hurdle exists by switching on a delicate many-body state called the Kondo effect. The Kondo effect manifests itself as a sharp resonance positioned a little above ε_f at temperatures around or lower than the so called Kondo temperature in the density of states of each impurity level. The Kondo temperature is usually governed by a low energy scale estimated to be

$$T_{K,g(e)} \simeq \left(\frac{D\Gamma}{4}\right)^{\frac{1}{2}} exp\left(-\frac{\pi|\varepsilon_{g(e)}|}{\Gamma}\right). \tag{22}$$

Here, D represents the half bandwidth of the density of states of the metal nanoparticles. The underlying action that is responsible for the build up of the Kondo resonance is the advent of simultaneous tunnelling of two electrons which have opposite spins at temperatures around or lower than $T_{K,g(e)}$. This singlet state creates the illusion of a spin flip at that energy level [30], breaking the Coulomb blockade, thus induces a current flow.

We will select the dipolar plasmon energy ε_p = 3.49 eV, the laser bandwidth δ = 1 meV and the coupling of the laser to the dipolar plasmon mode $\gamma = 2\pi|W_0|^2$ = 86 meV to facilitate comparison with previous work[23,24,27]. Left and right nanoparticles are fabricated from the same metal possessing identical parabolic density of states $\rho(\varepsilon)$ with half bandwidth $D = 9\Gamma$, where Γ = 0.8 eV. The left nanoparticle remains at environment temperature, i.e. $T_L = T$. Consequently, $T_{K,e}$ oscillates roughly between 23 K and 1.2 K while $T_{K,g} \approx 0$ since it is kept stationary. In the following discussion, T_K will refer to the Kondo temperature of $T_{K,e}$ at $t = 0$. The phonon frequency will be kept constant as $\omega_0 = 0.06\Gamma$ and λ will be adjusted to change the value of electron–phonon coupling strength $V_{e-p} = \lambda^2/\omega_0^2$.

We start our discussion with the evolution of the entropy current for two different ambient temperatures around T_K shown in Fig. 1. The data correspond to infinitesimal, low ($V \leq T_K$) and high bias ($V \geq 5\,T_K$) regimes at fixed electron–phonon coupling. The most obvious conclusion from this figure is that the entropy current oscillates with the same frequency as the driving gate voltage. The peak positions correspond to the case when ε_e is closest to ε_F and the trough positions correspond to the case when ε_e is farthest from ε_F as expected. However, the peak positions in infinitesimal and low bias regimes fall short of the peak position at $t = 0$, whereas this effect is far less pronounced at high bias regime.

Fig. 2 shows the evolution of the entropy current with a higher electron–phonon coupling with the other parameters the same as in Fig. 1. Here, it is clear that the oscillation amplitudes are smaller than Fig. 1 mainly because the peak of the oscillations is lower than the curves in Fig. 1 but this suppression is again less pronounced at high bias regime. It is also worth pointing out that in both Fig. 1 and Fig. 2, the instantaneous entropy current values are slightly higher in low bias regime than the infinitesimal bias one at $T = 2.4T_K$.

In order to test the effect of driving frequency on our results, we repeated the calculations in Fig. 1 by halving the driving frequency. The results are shown in Fig. 3, which clearly reveals that the peak position in the oscillations is now approaching the value at $t = 0$ for almost all bias values. Therefore, the amplitude of oscillations increases when the driving frequency is lowered. This implies that the instantaneous entropy current can attain higher peak values and reach the steady state maximum at $t = 0$ provided that sufficient time is allocated between the trough and peak positions of ε_e.

The results of our calculations are summarized in Fig. 4, where we show the amplitude of entropy current oscillations as a function of the bias voltage. We want to note that the amplitude is measured between successive peak and trough positions after skipping the initial steady state peak at $t = 0$. The results of further calculations with a driving frequency half of that in Fig. 3 are also included in Fig. 4. The peak locations of entropy current oscillations are almost equal to the

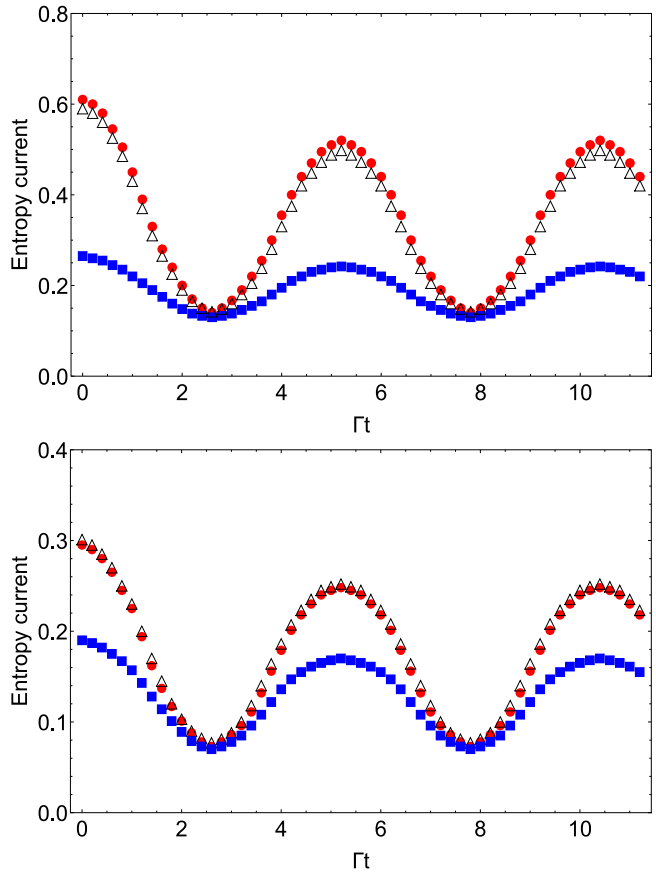

Fig. 1. Entropy current as a function of time for $V = 0.1\ T_K$ (red circles), $V = 0.7\ T_K$ (empty triangles) and $V = 6.2\ T_K$ (blue squares) with a temperature gradient of $\Delta T = 2$ K between the metal nanoparticles and assuming $\Delta = 40$ meV, $V_{e-p} = 2.25$ and $\omega = 0.384\pi\Gamma$ at $T = 0.7\ T_K$ (upper panel) and $T = 2.4\ T_K$ (lower panel).

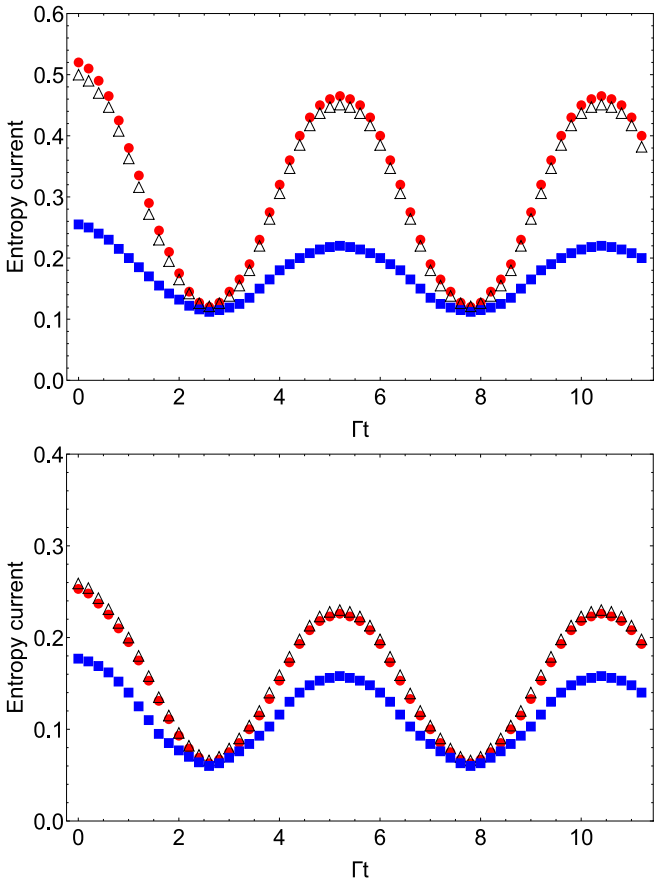

Fig. 2. Entropy current as a function of time at ambient temperature of $V = 0.1\ T_K$ (red circles), $V = 0.7\ T_K$ (empty triangles) and $V = 6.2\ T_K$ (blue squares) with a temperature gradient of $\Delta T = 2$ K between the metal nanoparticles assuming $\Delta = 40$ meV, $V_{e-p} = 3.75$ and $\omega = 0.384\pi\Gamma$ at $T = 0.7\ T_K$ (upper panel) and $T = 2.4\ T_K$ (lower panel).

steady state value at $t = 0$ indicating saturation. What is remarkable about these results is that the amplitude changes very little upon going from infinitesimal to low bias regime. This effect becomes even more discernible at $T = 2.4T_K$, where the amplitude is almost constant. Moreover, it is clear that reducing the electron–phonon coupling strength or the driving frequency has very little effect on the amplitude as well.

Therefore, there are two major effects that need to be discussed regarding these results. First one is the reduction of the amplitude in low bias regime in response to increasing the electron–phonon coupling strength at fixed driving frequency. This can be accounted for by recalling the role the Kondo resonance plays in quantum transport through this junction. Namely, the Kondo resonance enables to lift the Coulomb blockade, thereby facilitates the tunnelling between the left and right metal nanoparticles via the plasmon–exciton coupling. Since T_K at the trough position of the oscillation is roughly only 5% of T_K at the peak position, the Kondo resonance is quashed dramatically at the trough position. The main function of the electron–phonon coupling is to weaken the Kondo effect via the renormalization of the discrete state. Therefore, the suppression of the Kondo resonance is far more discernible at the peak position than the trough position because it is significantly more developed at the peak position. This results in an uneven quench of the entropy current at both ends of the oscillation cycle, thus we witness a reduction in the amplitude when the electron–phonon coupling strength is ramped up at fixed driving frequency. However, this trend is less noticeable at high bias regime because the Kondo resonance is already suppressed at the peak position due to the bias and this somewhat counters the uneven suppression at the peak and trough positions.

The second effect that needs to be elucidated is the amplification of the amplitude in response to decreasing driving frequency at low bias regime. In order to provide a credible explanation for this, we again need to comprehend the dynamical evolution of the Kondo resonance which crucially determines the real time behaviour of the entropy current. It is well known that the full development of the Kondo resonance takes a significant amount of time [31,32], so that the fast modulation of ϵ_e prevents it from spending sufficient time when it moves from the trough position to the peak position. This, in turn, hampers the full development of the Kondo resonance at the peak position. When the Kondo resonance cannot reach its full prominence at the peak position, neither can the entropy current reach its steady state value at $t = 0$. This is the underlying reason for the reduction of the amplitude in low bias regime. As for the high bias regime, the Kondo resonance once again loses much of its prominence at the peak position. Therefore, reducing the driving frequency is not sufficient by itself for the Kondo resonance to develop fully. This manifests itself as a far more gradual increase in amplitude upon decreasing the driving frequency than the low bias regime. We also would like to point out that reducing the driving frequency below the lowest one in Fig. 4, i.e. $\omega = 0.096\pi\Gamma$, no longer changes the amplitudes and the peak positions in oscillations roughly match the steady state at $t = 0$. This implies that the Kondo resonance manages to gain full prominence because ϵ_e is allocated sufficiently long time to go from the trough position to peak position.

Finally, we show in Fig. 5 the steady state entropy current values at $t = 0$ for a wide range of bias values at the same temperatures

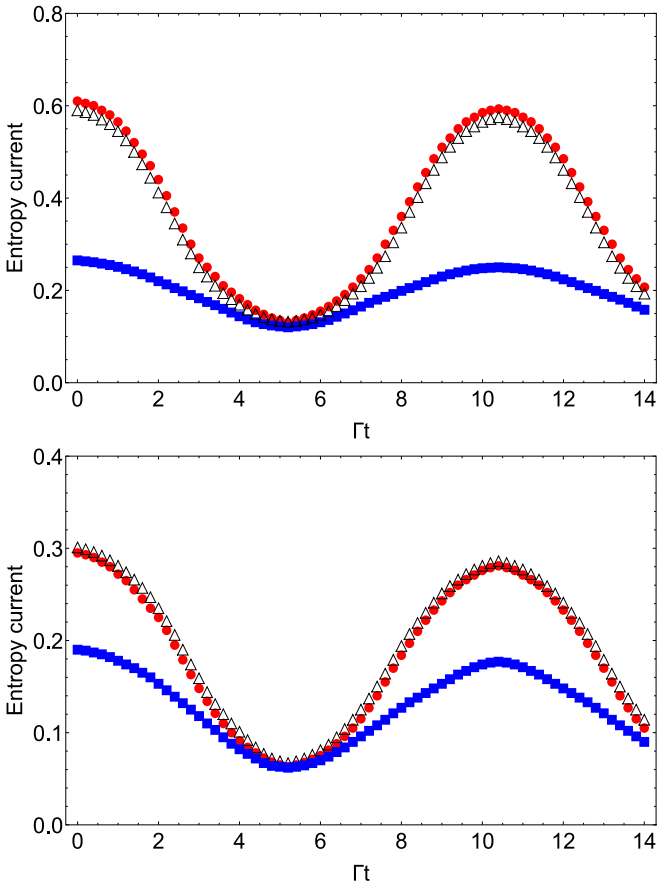

Fig. 3. Entropy current as a function of time at ambient temperature of $V = 0.1\ T_K$ (red circles), $V = 0.7\ T_K$ (empty triangles) and $V = 6.2\ T_K$ (blue squares) with a finite temperature gradient of $\Delta T = 2$ K between the metal nanoparticles assuming a plasmon–exciton coupling strength $\Delta = 40$ meV for $V_{e-p} = 2.25$ and $\omega = 0.192\pi\Gamma$ at $T = 0.7\ T_K$ (upper panel) and $T = 2.4\ T_K$ (lower panel).

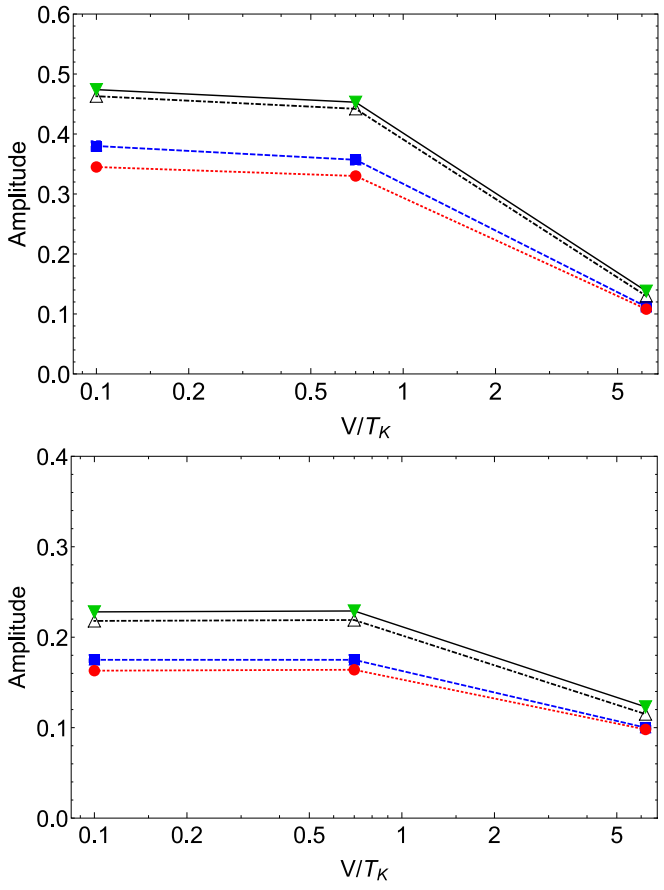

Fig. 4. The amplitude of the oscillations in entropy current as a function of voltage bias at $V_{e-p} = 3.75$ and $\omega = 0.384\pi\Gamma$ (red circles), $V_{e-p} = 2.25$ and $\omega = 0.384\pi\Gamma$ (blue squares), $V_{e-p} = 2.25$ and $\omega = 0.192\pi\Gamma$ (empty triangles), $V_{e-p} = 2.25$ and $\omega = 0.096\pi\Gamma$ (green inverted triangles) with a finite temperature gradient of $\Delta T = 2$ K between the metal nanoparticles assuming a plasmon–exciton coupling strength $\Delta = 40$ meV is shown for $T = 0.7\ T_K$ (upper panel) and for $T = 2.4\ T_K$ (lower panel).

and electron–phonon coupling strengths used in earlier time-dependent calculations. These results supplement the previous calculations carried out without electron–phonon coupling. A general equation governing the behaviour of the entropy current is expressed as

$$I^s = \frac{I_R^h}{T_R} = \frac{\Delta T G L T}{T - \Delta T}, \tag{23}$$

where G denotes the electrical conductance and L represents the Lorentz number [23]. It is important to note that the actual value of L can differ from the textbook value $L_0 = \frac{\pi^2 k_B^2}{3e^2}$ considerably.

There are two peculiarities that need to be addressed in Fig. 5. First, the entropy current converges to a small value when $V \geq 50 T_K$ despite the fact that the Kondo resonance is almost entirely washed way, thus G is vanishingly small. In this regime, positive large nonlinear modifications to L [23] compensate the diminishing G to sustain a finite entropy current. Second, the entropy current is quenched more in low bias regime ($V \leq T_K$) compared to the high bias regime ($V \geq 5\ T_K$) as a result of the electron–phonon coupling. In order to account for this, we should recall that the action of the electron–phonon coupling is to suppress the Kondo resonance by pushing ε_e lower via renormalization. Therefore, its role is far more discernible in the low bias regime, where the Kondo resonance is fully developed. On the other hand, the Kondo resonance is diminished in high bias regime. This implies that there is not much left to be annihilated anyway. Moreover, the value of L is also larger in high bias regime because of the nonlinear corrections [23]. The combination of these factors enables the entropy current to stay resilient in high bias regime upon boosting the electron–phonon coupling.

4. Conclusions

In conclusion, we believe that our accurate and realistic portrayal of quantum thermodynamic behaviour of a plexcitonic nanojunction holds great promise to design state-of-the-art novel photovoltaic devices that will hopefully exceed the Shockley–Queisser limit in near future. From an experimental point of view, we think that a slight adjustment in the intensity of the laser beam would be sufficient to generate a temperature gradient across the plasmonic nanojunction and the sinusoidal modulation of a discrete state can be achieved by attaching a gate voltage to the quantum emitter. Our aim is, then, to spur new experiments in the exciting fields of quantum plasmonics and solar photovoltaics with the intriguing results presented in this paper. We also plan to investigate the effect of contact material in the future [33].

The data that support the findings of this study are available from the corresponding author upon reasonable request.

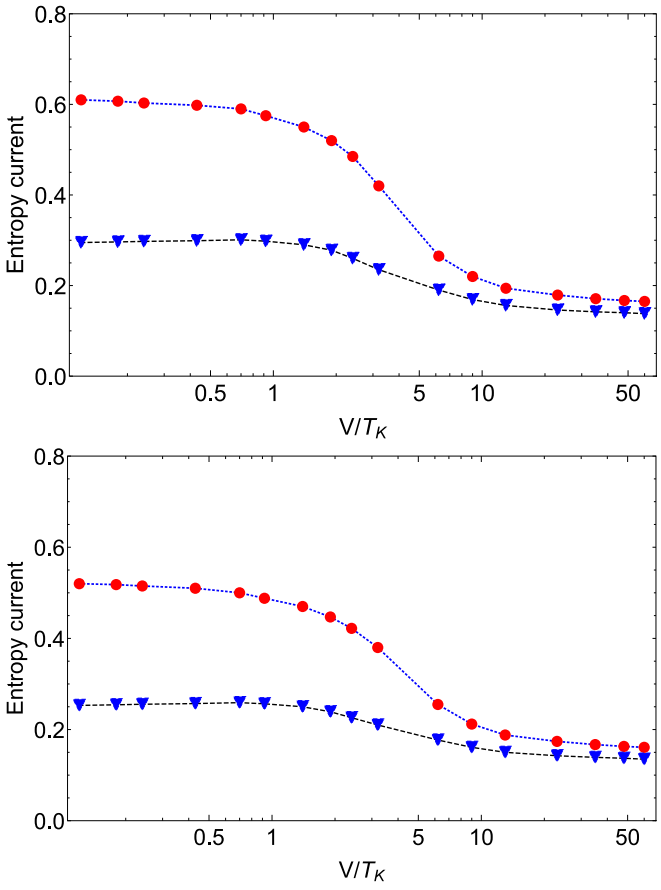

Fig. 5. Entropy current as a function of the voltage bias at ambient temperature of $T = 0.7\ T_K$ (red circles), $T = 2.4\ T_K$ (blue inverted triangles) with a finite temperature gradient of $\Delta T = 2$ K between the metal nanoparticles assuming a plasmon–exciton coupling strength $\Delta = 40$ meV with electron phonon coupling $V_{e-p} = 2.25$ (upper panel) and $V_{e-p} = 3.75$ (lower panel).

CRediT authorship contribution statement

A. Goker: Conceptualization, Methodology, Software, Writing – review & editing.

Declaration of competing interest

The authors declare that they have no known competing financial interests or personal relationships that could have appeared to influence the work reported in this paper.

References

[1] M.A. Kastner, The single-electron transistor, Rev. Modern Phys. 64 (1992) 849.
[2] P. Avouris, Z. Chen, V. Perebeinos, Carbon based electronics, Nature Nanotech. 2 (2007) 605–615.
[3] M.S. Tame, K.R. McEnery, S.K. Özdemir, J. Lee, S.A. Maier, M.S. Kim, Quantum plasmonics, Nat. Phys. 9 (2013) 329–340.
[4] S.A. Maier, P.G. Kik, H.A. Atwater, S. Meltzer, E. Harel, B.E. Koel, A.G. Requicha, Local detection of electromagnetic energy transport below the diffraction limit in metal nanoparticle plasmon waveguides, Nature Mater. 2 (2003) 229–232.
[5] J.A. Schuller, E.S. Barnard, W. Cai, Y.C. Jun, J.S. White, M.L. Brongersma, Plasmonics for extreme light concentration and manipulation, Nature Mater. 9 (2010) 193–204.
[6] F. Wang, Y.R. Shen, General properties of local plasmons in metal nanostructures, Phys. Rev. Lett. 97 (2006) 206806.
[7] G.A. Wurtz, P.R. Evans, W. Hendren, R. Atkinson, W. Dickson, R.J. Pollard, A.V. Zayats, W. Harrison, C. Bower, Molecular plasmonics with tunable exciton-plasmon coupling strength in j-aggregate hybridized au nanorod assemblies, Nano Lett. 7 (2007) 1297–1303.
[8] R. Yang, Y. Cheng, Y. Song, V.I. Belotelov, M. Sun, Plasmon and plexciton driven interfacial catalytic reactions, Chem. Record 21 (2021) 797–819.
[9] H.A. Atwater, A. Polman, Plasmonics for improved photovoltaic devices, Nature Mater. 9 (2010) 205–213.
[10] K.R. Catchpole, A. Polman, Plasmonic solar cells, Opt. Express 16 (2008) 21793–21800.
[11] J. Lee, A.O. Govorov, J. Dulka, N.A. Kotov, Bioconjugates of CdTe nanowires and Au nanoparticles: Plasmon-exciton interactions, luminescence enhancement and collective effects, Nano Lett. 4 (2004) 2323–2330.
[12] S.K. Cushing, N. Wu, Progress and perspectives of plasmon-enhanced solar energy conversion, J. Phys. Chem. Lett. 7 (2016) 666–675.
[13] J. Li, S.K. Cushing, F. Meng, T.R. Senty, A.D. Bristow, N. Wu, Plasmon-induced resonance energy transfer for solar energy conversion, Nature Photon. 9 (2015) 601–607.
[14] C. Sönnichsen, T. Franzl, T. Wilk, G. von Plessen, J. Feldmann, O. Wilson, P. Mulvaney, Drastic reduction of plasmon damping in gold nanorods, Phys. Rev. Lett. 88 (2002) 077402.
[15] R.Q. Li, F.J. Garcia-Vidal, A.I. Fernandez-Dominguez, Plasmon-exciton coupling in symmetry-broken nanocavities, ACS Photonics 5 (2018) 177–185.
[16] A. Delga, J. Feist, J. Bravo-Abad, F.J. Garcia-Vidal, Quantum emitters near a metal nanoparticle: strong coupling and quenching, Phys. Rev. Lett. 112 (2014) 253601.
[17] D.E. Gomez, H. Giessen, T.J. Davis, Semiclassical plexcitonics: Simple approach for designing plexcitonic nanoparticles, J. Phys. Chem. C 118 (2014) 23963–23969.
[18] S. Wang, G.D. Scholes, L.Y. Hsu, Quantum dynamics of a molecular emitter strongly coupled with surface plasmon polaritons: A macroscopic quantum electrodynamics approach, J. Chem. Phys. 151 (2019) 014105.
[19] A. Delga, J. Feist, J. Bravo-Abad, F.J. Garcia-Vidal, Theory of strong coupling between quantum emitters and localized surface plasmons, J. Opt. 16 (2014) 114018 (1–8).
[20] X. Mu, M. Sun, Interfacial charge transfer exciton enhanced by plasmon in 2D in-plane lateral and van der Waals heterostructures, Appl. Phys. Lett. 117 (2020) 091601.
[21] A. Goker, Strongly correlated plexcitonics: evolution of the Fano resonance in the presence of Kondo correlations, Phys. Chem. Chem. Phys. 17 (2015) 11569–11576.
[22] A. Goker, H. Aksu, Quantum transport through a Coulomb blockaded quantum emitter coupled to a plasmonic dimer, Phys. Chem. Chem. Phys. 18 (2016) 1980–1991.
[23] A. Goker, Entropy current through a strongly correlated plexcitonic nanojunction, J. Phys. Chem. C 122 (2018) 4607–4614.
[24] A. Goker, H. Aksu, B.D. Dunietz, Heat flow enhancement in a nanoscale plasmonic junction induced by kondo resonances and electron-phonon coupling, Physica E 127 (2021) 114536.
[25] A. Goker, Kondo resonance in an AC driven quantum dot subjected to finite bias, Solid State Commun. 148 (2008) 230.
[26] I.G. Lang, Y.A. Firsov, Kinetic theory of semiconductors with low mobility, JETP 16 (1963) 1301–1312.
[27] A. Manjavacas, F.J. Garcia de Abajo, P. Nordlander, Quantum plexcitonics: Strongly interacting plasmons and excitons, Nano Lett. 11 (2011) 2318–2323.
[28] L. Cui, W. Jeong, S. Hur, M. Matt, J.C. Klockner, F. Pauly, P. Nielaba, J.C. Cuevas, E. Meyhofer, P. Reddy, Quantized thermal transport in single atom junctions, Science 355 (2017) 1192–1195.
[29] L. Cui, S. Hur, Z.A. Akbar, J.C. Klockner, W. Jeong, F. Pauly, S.Y. Jang, P. Reddy, E. Meyhofer, Thermal conductance of single molecule junctions, Nature 572 (2019) 628–633.
[30] J. Kondo, Resistance minimum in dilute magnetic alloys, Progr. Theoret. Phys. 32 (1964) 37.
[31] P. Nordlander, M. Pustilnik, Y. Meir, N.S. Wingreen, D.C. Langreth, How long does it take for the kondo effect to develop? Phys. Rev. Lett. 83 (1999) 808–811.
[32] M. Plihal, D.C. Langreth, P. Nordlander, Transient currents and universal timescales for a fully time-dependent quantum dot in the Kondo regime, Phys. Rev. B 71 (2005) 165321.
[33] A. Goker, E. Gedik, Designer thermal switches: the effect of the contact material on instantaneous thermoelectric transport through a strongly interacting quantum dot, J. Phys.: Condens. Matter 25 (2013) 365301.